18th International Conference
ENGINEERING MECHANICS 2012
Svratka, Czech Republic, May 14 – 17, 2012

pp. 1555–1564
Paper #28

NUMERICAL MODELLING OF ENGINEERED CEMENT-BASED COMPOSITES

J. Vorel [*], **W.P. Boshoff** [**]

Abstract: *Strain Hardening Cement-based Composite (SHCC) is a type of High Performance Concrete (HPC) that was developed to overcome the brittleness of conventional concrete. Even though there is no significant compressive strength increase compared to conventional concrete, it exhibits superior behavior in tension. The primary objective of the presented research is to develop a constitutive model that can be used to simulate structural components with SHCC under different types of loading conditions.*

Keywords: ***Strain Hardening Cement-based Composite (SHCC), rotating crack model, damage, cyclic loading, nonlinear unloading***

1. Introduction

Strain Hardening Cement-based Composite (SHCC) is a type of High Performance Concrete (HPC) that was developed to overcome the brittleness of conventional concrete. Even though there is no significant compressive strength increase compared to conventional concrete, it exhibits superior behavior in tension. It has been shown to reach a tensile strain capacity of more than 4% during a pseudo strain hardening phase (Li and Wang, 2001; Boshoff and van Zijl, 2007). This pseudo strain hardening is achieved by the formation of fine, closely spaced multiple cracks with crack widths normally not exceeding $100\mu m$ (Li and Wang, 2001). These fine cracks, compared to large (larger than $100\mu m$) localized cracks found in conventional concrete, have the advantage of increased durability. For a further discussion of the mechanical properties of SHCC, the reader is referred to (Boshoff *et al.*, 2009*a*,*b*).

Several scholars have simulated SHCC mechanical behavior with the Finite Element Method (FEM). Kabele (2000) formulated a model to simulate the mechanical behavior of SHCC using a smeared cracking approach. Despite acknowledging that a discrete cracking model would be best for the final localizing crack, Kabele decided to use a smeared cracking approach for the localization. This is due to the uncertainty of the position of the final localizing crack. Another model was proposed by Han *et al.* (2003). This model was created to simulate the behavior of SHCC under cyclic loading to test the improvement of structural response if SHCC elements are used to dissipate energy during earth-quake loadings. Computational modeling of SHCC was also performed by Simone *et al.* (2003) who used an embedded discontinuity approach for the final material softening. This method would have the same kinematic characterization as one obtained with interface elements for discrete cracking, but does not require remeshing procedures. Their conclusion was that it did not simulate the experimental results of SHCC satisfactorily due to the simplicity of the model.

Boshoff (2007) created a simple damage mechanics based model for the tensile behavior of SHCC. This was implemented numerically using the FEM. Even though numerous shortcomings still exist, the model showed relatively good results. Remaining issues include an unresolved mesh dependence and the under prediction of the deformation when analyzing a structure with a strain gradient.

The primary objective of the presented research is to develop a constitutive model that can be used to simulate structural components with SHCC under different types of loading conditions. In particular, the constitutive model must be efficient and robust for large-scale simulations while restricted number

[*]Ing. Jan Vorel, Ph.D.: Department of Mechanics, Faculty of Civil Engineering, Czech Technical University in Prague, Thákurova 7; 166 29, Prague; CZ, e-mail: jan.vorel@fsv.cvut.cz
[**]Dr William Peter Boshoff: Stellenbosch University, Department of Civil Engineering; Private Bag X1 Matieland 7602; South Africa, e-mail: bboshoff@sun.ac.za

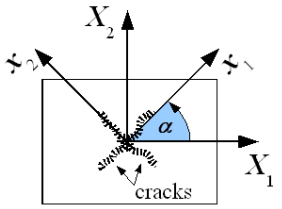

Fig. 1: Coordinates and transformation angle

of material parameters is needed. The proposed model for plane stress is outlined and the results of the preliminary implementation are shown.

2. Model definition

For the modeling of specific behavior of SHCC in tension, the application of classical constitutive material models used for quasi-brittle materials is not straightforward. The proposed numerical model is based on a rotating crack assumption to capture specific characteristics of SHCC, i.e. the strain hardening and softening, the multiple cracking and the crack localization. Multiple orthogonal crack patterns are allowed which is in accordance with the observations presented by Suryanto *et al.* (2008). A schematic representation of orthogonal cracking using the rotating crack model is shown using global and local axes in Fig. 1. A complete description of the rotating crack model can be found in (Rots, 1998).

The presented model is implemented in a commercially available software package, **DIANA** (BV., 2008), for a plane stress elements using a coaxial rotating crack model (RCM) with two orthogonal cracks as described in (Han *et al.*, 2003). This numerical approach is classified as the smeared cracking approach. When implementing the model into a nonlinear fine element code, the incremental-iterative procedure based on a strain increment is assumed. Therefore, the strain vector $\boldsymbol{\varepsilon} = \{\varepsilon_{11}, \varepsilon_{22}, \gamma_{12}\}^{\mathsf{T}}$ reads

$$\boldsymbol{\varepsilon}^{(i)} = \boldsymbol{\varepsilon}^{(i-1)} + \Delta\boldsymbol{\varepsilon}, \tag{1}$$

where i stands for an increment number and $\Delta\boldsymbol{\varepsilon}$ is a strain increment vector. The rotating crack model evaluates a given strain state and generates the inelastic strain in the principal directions of the strain. Therefore, it is inevitably required to introduce a transformation tensor $([\mathsf{T}]_{\varepsilon}, [\mathsf{T}]_{\sigma})$ interconnecting global and a principal strain $\mathbf{e} = \{e_1, e_2, 0\}^{\mathsf{T}}$ or stress $\mathbf{s} = \{s_1, s_2, 0\}^{\mathsf{T}}$, respectively

$$\mathbf{e} = [\mathsf{T}]_{\varepsilon}\,\boldsymbol{\varepsilon}, \quad \mathbf{s} = [\mathsf{T}]_{\sigma}\,\boldsymbol{\sigma}. \tag{2}$$

Using the standard transformation rule the tensors are

$$[\mathsf{T}]_{\varepsilon} = \begin{bmatrix} n_{11}^2 & n_{12}^2 & n_{11}n_{12} \\ n_{21}^2 & n_{22}^2 & n_{21}n_{22} \\ 2n_{11}n_{21} & 2n_{12}n_{22} & n_{11}n_{22} + n_{12}n_{21} \end{bmatrix}, \tag{3}$$

$$\boldsymbol{n} = \begin{bmatrix} \cos\alpha & \sin\alpha \\ -\sin\alpha & \cos\alpha \end{bmatrix}, \tag{4}$$

with the relations between $[\mathsf{T}_{\varepsilon}]$ and $[\mathsf{T}_{\sigma}]$

$$[\mathsf{T}]_{\sigma}{}^{\mathsf{T}} = [\mathsf{T}]_{\varepsilon}{}^{-1} \quad \text{and} \quad [\mathsf{T}]_{\varepsilon}{}^{\mathsf{T}} = [\mathsf{T}]_{\sigma}{}^{-1}. \tag{5}$$

The rotation angle α can be obtained by means of a standard relation

$$\alpha = 1/2 \arctan\left[\gamma_{12}/\left(\varepsilon_{11} - \varepsilon_{22}\right)\right]. \tag{6}$$

The incremental stress-strain law (in the crack orientation) reads

$$\Delta \mathbf{s} = [\tilde{\mathsf{D}}]\Delta \mathbf{e}, \tag{7}$$

$$[\tilde{\mathsf{D}}] = \begin{bmatrix} \frac{\mathrm{d}s_1}{\mathrm{d}e_1} & \frac{\mathrm{d}s_1}{\mathrm{d}e_2} & 0 \\ \frac{\mathrm{d}s_2}{\mathrm{d}e_1} & \frac{\mathrm{d}s_2}{\mathrm{d}e_2} & 0 \\ 0 & 0 & \frac{s_1 - s_2}{2(e_1 - e_2)} \end{bmatrix}, \tag{8}$$

where $[\tilde{\mathsf{D}}]$ is the tangent material stiffness matrix. The derivation can be found in (Jirásek and Zimmermann, 1998). The stiffness matrix is transformed to the global coordinates using the standard transformation rule

$$[\mathsf{D}] = [\mathsf{T}_\varepsilon]^{\mathsf{T}} [\tilde{\mathsf{D}}] [\mathsf{T}_\varepsilon]. \tag{9}$$

2.1. Poisson's ratio effect and equivalent principal stresses

It has to be mentioned that the rotating crack approach does not automatically include the effect of Poisson's ratio as the stress is evaluated on the basis of individual principal strains. In (Han *et al.*, 2003) the definition of equivalent strain is used to take this effect into account. This approach is reliable when a model formulation does not permit residual deformations by cyclic loading, i.e. by changing state (tension to compression and vice versa). However, in the model presented in this study permanent (residual) deformations are allowed. Therefore, a new approach was employed to treat the effect of Poisson's ratio. The effective principal strain $(\hat{\mathbf{e}})$ is used to determine the equivalent stress $(\hat{\mathbf{s}})$ from the simplified uniaxial stress-strain diagram (see Sec. 2.2.). The effective principal strain is based on the principal strain $(\mathbf{e})$ which is free of inelastic deformations caused during the stress state change. The final stresses are consequently evaluated as

$$\begin{Bmatrix} s_1 \\ s_2 \end{Bmatrix} = \frac{1}{1 - \nu_{12}\nu_{21}} \begin{bmatrix} 1 & \nu_{12} \\ \nu_{21} & 1 \end{bmatrix} \begin{Bmatrix} \hat{s}_1 \\ \hat{s}_2 \end{Bmatrix}, \tag{10}$$

$$\nu_{12} = \nu_0 E_1 / E_0, \quad \nu_{21} = \nu_0 E_2 / E_0, \tag{11}$$

where E_0 and ν_0 stand for Young's modulus and Poisson's ratio of the undamaged material respectively. The parameters E_1, E_2, ν_{12} and ν_{21} represent the characteristics of the damaged material in a given direction and are defined in Sec. 2.2.. The isotropic elastic material is represented in the state without cracks ($E_1 = E_2 = E_0$, $\nu_{12} = \nu_{21} = \nu_0$) and the orthotropic when the crushing or cracking starts

$$\{\hat{s}_1, \hat{s}_2\}^{\mathsf{T}} = \left\{E_1 e_1^{\mathsf{el}}, E_2 e_2^{\mathsf{el}}\right\}^{\mathsf{T}}. \tag{12}$$

Stiffness matrix introduced with this approach satisfies the condition of symmetry for orthotropic materials. Combining Eqs. (10,12) further gives

$$\begin{Bmatrix} s_1 \\ s_2 \end{Bmatrix} = \frac{1}{1 - \nu_{12}\nu_{21}} \begin{bmatrix} E_1 & \nu_{12}E_2 \\ \nu_{21}E_1 & E_2 \end{bmatrix} \begin{Bmatrix} e_1^{\mathsf{el}} \\ e_2^{\mathsf{el}} \end{Bmatrix}, \tag{13}$$

where $\nu_{12}E_2 = \nu_{21}E_1$ and superscript $\cdot^{\mathsf{el}}$ represents the elastic part.

2.2. Equivalent stress

The equivalent stress state in principal direction is determined by the stress function $\hat{s}_{t(c)}$ as a function of the current principal strain and associated history parameters.

The stress function is based on the uniaxial strain-stress diagrams in compression and tension. The experimental data are idealized to obtain a suitable mathematical representation of this constitutive model.

Tension

The material response for virgin loading in tension (Fig. 2(a)) is described for each individual part by

$$\hat{s}_t\left(\hat{e} \geq \varepsilon_{tmax}\right) = \begin{cases} E_0 \hat{e} & 0 \leq \hat{e} \leq \varepsilon_{t0} \\ \sigma_{t0} + \left(\sigma_{tp} - \sigma_{t0}\right)\left[-2\left(\frac{\hat{e}-\varepsilon_{t0}}{\varepsilon_{tp}-\varepsilon_{t0}}\right)^3 + 3\left(\frac{\hat{e}-\varepsilon_{t0}}{\varepsilon_{tp}-\varepsilon_{t0}}\right)^2\right] & \varepsilon_{t0} < \hat{e} \leq \varepsilon_{tp} \\ \sigma_{tp}\left[2\left(\frac{\hat{e}-\varepsilon_{tp}}{\varepsilon_{tu}-\varepsilon_{tp}}\right)^3 - 3\left(\frac{\hat{e}-\varepsilon_{tp}}{\varepsilon_{tu}-\varepsilon_{tp}}\right)^2 + 1\right] & \varepsilon_{tp} < \hat{e} < \varepsilon_{tu} \\ 0 & \varepsilon_{tu} \leq \hat{e}. \end{cases} \tag{14}$$

The model parameters are depicted in Fig. 2(a). The elastic part is assumed to be linear whereas the hardening and the softening sections are defined by means of the Hermit functions.

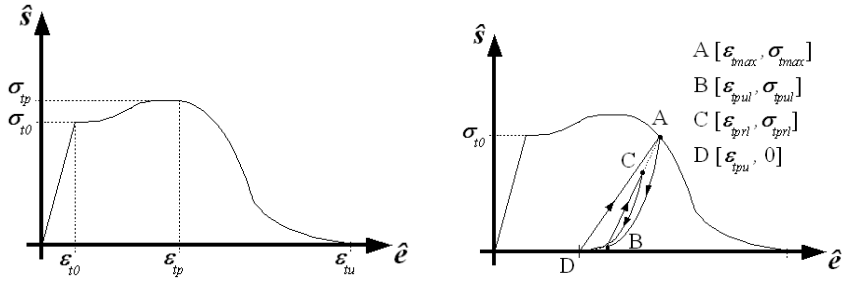

(a) (b)

Fig. 2: Tensile response: (a) Virgin loading, (b) loading/unloading

The unloading and reloading scheme shown in Fig. 2(b) is based on the experiments presented by Mechtcherine and Jůn (2007).

$$\hat{s}_t\left(\hat{e} < \varepsilon_{tmax}\right) = \begin{cases} E_0 \hat{e} & 0 \leq \varepsilon_{tmax} \leq \varepsilon_{t0} \\ \sigma^*_{tmax}\left(\frac{\hat{e}-\varepsilon_{tul}}{\varepsilon^*_{tmax}-\varepsilon_{tul}}\right)^{a_t} & \varepsilon_{t0} < \varepsilon_{tmax} < \varepsilon_{tu}, \dot{e} < 0 \\ \sigma^*_{tul} + \left(\sigma_{tmax} - \sigma^*_{tul}\right)\frac{\hat{e}-\varepsilon^*_{tul}}{\varepsilon_{tmax}-\varepsilon^*_{tul}} & \varepsilon_{t0} < \varepsilon_{tmax} < \varepsilon_{tu}, \dot{e} \geq 0 \\ 0 & \varepsilon_{tu} \leq \varepsilon_{tmax}. \end{cases} \tag{15}$$

The unloading curve is based on the polynomial function and the reloading is assumed to be linear. The partial unloading and reloading is incorporated using

$$\begin{aligned} \varepsilon^*_{tmax} &= \min\left(\varepsilon_{tmax}, \varepsilon_{tprl}\right), \\ \varepsilon^*_{tul} &= \max\left(\varepsilon_{tul}, \varepsilon_{tpul}\right), \end{aligned} \tag{16}$$

where $\sigma^*_{tmax}, \sigma^*_{tul}$ are associated stresses and ε_{tmax} is the maximum strain experienced in previous steps with stress σ_{tmax}. The evolution of inelastic strain ε_{tul} is assumed to be linearly dependent on ε_{tmax} for the elastic and hardening part and linearly dependent on the crack opening for the softening branch (Eq. (17)). This simplification correlates well with recent, unpublished cyclic tensile results done at Stellenbosch University, see Fig. 3(a).

$$\varepsilon_{tul} = \begin{cases} 0 & 0 \leq \varepsilon_{tmax} \leq \varepsilon_{t0} \\ b_t\left(\varepsilon_{tmax} - \varepsilon_{t0}\right) & \varepsilon_{t0} < \varepsilon_{tmax} \leq \varepsilon_{tp} \\ \min\left\{b_t\left(\varepsilon_{tp} - \varepsilon_{t0}\right) + b_t\left[\varepsilon_{tmax} - b_t\left(\varepsilon_{tp} - \varepsilon_{t0}\right) - \sigma_{tmax}/E_{tp}\right], \right. & \\ \left. b_t\left(\varepsilon_{tp} - \varepsilon_{t0} + w_t/h\right)\right\} & \varepsilon_{tp} < \varepsilon_{tmax}, \end{cases} \tag{17}$$

where $E_{tp} = \sigma_{tp}/\left[\varepsilon_{tp} - b_t(\varepsilon_{tp} - \varepsilon_{t0})\right]$. The parameter a_t governs the unloading trajectory and must be determined from the experimental tests as well as the material characteristic b_t.

To ensure proper energy dissipation during localizing, the crack band approach is used which relates the strain ε_{tu} to the crack opening for the complete force transfer loss (w_t) and element size (h), see

Eq. (18). The crack opening can be considered as a half of the fiber length (Boshoff, 2007). In the present study the equivalent crack band width is evaluated by projecting the element into the direction normal to the crack at its initiation (h). This is done for each cracking direction separately. The last term in Eq. (18) describes the influence of the unloading where more energy is dissipated when the non-linear law is employed (Fig. 3(b)).

$$\varepsilon_{tu} = \varepsilon_{tp} + \frac{w_t}{h} - 2\frac{\varepsilon_{tp} - b_t\left(\varepsilon_{tp} - \varepsilon_{t0}\right)}{a_t + 1}. \tag{18}$$

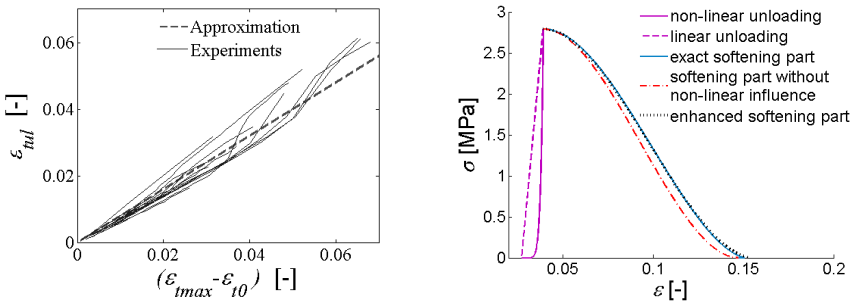

(a) (b)

Fig. 3: Tension: (a) Evolution of inelastic strain, (b) comparison of softening branches

As seen in Eq. (17), the damage and cracking strains are mainly driven by a single material parameter, namely b_t. By considering the standard definition of the damage parameter ω

$$E_t = (1 - \omega_t)E_0, \tag{19}$$

where E_t denotes the actual elastic modulus, the damage variable can be determined by introducing Eq. (17) into Eq. (19) as

$$\omega_t = 1 - \frac{E_t}{E_0} = 1 - \frac{\sigma_{tmax}}{\left(\varepsilon_{tmax} - \varepsilon_{tul}\right)E_0}. \tag{20}$$

The transverse strain ratio in Eq. (11) can be then evaluated as

$$\nu_{ij} = -\nu_0\left(1 - \omega_t\right). \tag{21}$$

This definition assures the decreasing influence of Poisson's ratio while the material cracks.

Compression

The virgin compression loading response is shown in Fig. 4(a) and is defined mathematically as

$$\hat{s}_c\left(\hat{e} \leq \varepsilon_{min}\right) = \begin{cases} E_0\hat{e} & 0 > \hat{e} \geq \varepsilon_{c0} \\ \sigma_{cp} - \left(\sigma_{cp} - \sigma_{c0}\right)\left(\frac{\varepsilon_{cp}-\hat{e}}{\varepsilon_{cp}-\varepsilon_{c0}}\right)^{E_0\frac{\varepsilon_{cp}-\varepsilon_{c0}}{\sigma_{cp}-\sigma_{c0}}} & \varepsilon_{c0} > \hat{e} \geq \varepsilon_{cp} \\ \sigma_{cp}\left[2\left(\frac{\hat{e}-\varepsilon_{cp}}{\varepsilon_{cu}-\varepsilon_{cp}}\right)^3 - 3\left(\frac{\hat{e}-\varepsilon_{cp}}{\varepsilon_{cu}-\varepsilon_{cp}}\right)^2 + 1\right] & \varepsilon_{cp} > \hat{e} > \varepsilon_{cu} \\ 0 & \varepsilon_{cu} \geq \hat{e}. \end{cases} \tag{22}$$

The unloading and reloading scheme is depicted in Fig. 4(b) and is based on a similar assumptions as for tension

$$\hat{s}_c\left(\hat{e} > \varepsilon_{cmin}\right) = \begin{cases} E_0\hat{e} & 0 > \varepsilon_{cmin} \geq \varepsilon_{t0} \\ \sigma^*_{cmin}\left(\frac{\hat{e}-\varepsilon_{cul}}{\varepsilon^*_{cmin}-\varepsilon_{cul}}\right)^{a_c} & \varepsilon_{c0} > \varepsilon_{cmin} > \varepsilon_{cu}, \dot{e} > 0 \\ \sigma^*_{cul} + \left(\sigma_{cmin} - \sigma^*_{cul}\right)\frac{\hat{e}-\varepsilon^*_{cul}}{\varepsilon_{cmin}-\varepsilon^*_{cul}} & \varepsilon_{c0} > \varepsilon_{cmin} > \varepsilon_{cu}, \dot{e} \leq 0 \\ 0 & \varepsilon_{cu} \geq \varepsilon_{cmin}, \end{cases} \tag{23}$$

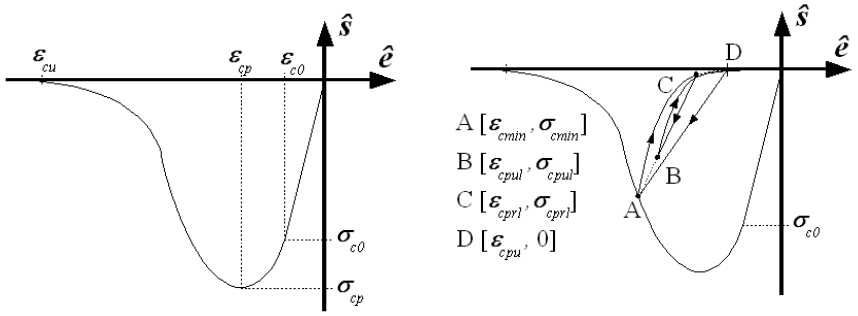

(a) (b)

Fig. 4: Compressive response: (a) Virgin loading, (b) loading/unloading

where

$$\begin{aligned} \varepsilon^*_{cmin} &= \max\left(\varepsilon_{cmin}, \varepsilon_{cprl}\right), \\ \varepsilon^*_{cul} &= \min\left(\varepsilon_{cul}, \varepsilon_{cpul}\right). \end{aligned} \tag{24}$$

where $\sigma^*_{cmin}, \sigma^*_{cul}$ are associated stresses and ε_{cmin} is the minimum strain reached in previous steps with stress σ_{cmin}. The evolution of inelastic strain is again assumed to be linearly dependent on ε_{cmin} and crushing (Eq. (25)). Suppose that the strain $\left(\varepsilon^{test}_{cu}\right)$ for which the force is totally released is determined from the experimental test and the corresponding localisation band in real material is denoted d_c. Next, with the knowledge of the remaining material parameters, we can define the displacement needed for releasing correct energy during material softening as $w_c = \left[\varepsilon^{test}_{cu} - b_c\left(\varepsilon_{cp} - \varepsilon_{c0}\right)\right] d_c$. The inelastic strain then takes the form

$$\varepsilon_{cul} = \begin{cases} 0 & 0 > \varepsilon_{cmin} \geq \varepsilon_{c0} \\ b_c\left(\varepsilon_{cmin} - \varepsilon_{c0}\right) & \varepsilon_{c0} > \varepsilon_{cmin} \geq \varepsilon_{cp} \\ \min\left\{b_c\left(\varepsilon_{cp} - \varepsilon_{c0}\right) + b_c\left[\varepsilon_{cmin} - b_c\left(\varepsilon_{cp} - \varepsilon_{c0}\right) - \sigma_{cmin}/E_{cp}\right], \right. & \\ \left. b_c\left(\varepsilon_{cp} - \varepsilon_{c0} + w_c/h\right)\right\} & \varepsilon_{cp} > \varepsilon_{cmin}. \end{cases} \tag{25}$$

The material parameters a_c and b_c have to be determined from experimental test results.

The dissipated energy during the crushing should also be mesh-independent as for tensile cracking. Therefore, the strain ε_{cu} is defined with respect to the mesh size as

$$\varepsilon_{cu} = \varepsilon_{cp} + \frac{w_c}{h} - 2\frac{\varepsilon_{cp} - b_c\left(\varepsilon_{cp} - \varepsilon_{c0}\right)}{a_c + 1}, \tag{26}$$

where h represents the equivalent band (element size) where the crushing occurs and is determined at its initiation. The damage parameter is determined in a similar fashion as for tension (Eq. (20)) and reads

$$\omega_c = 1 - \frac{E_c}{E_0} = 1 - \frac{\sigma_{cmin}}{\left(\varepsilon_{cmin} - \varepsilon_{cul}\right) E_0}. \tag{27}$$

2.3. Biaxial behavior

To demonstrate the complex behavior of the proposed approach the failure envelope in space of principal stresses is shown in Fig. 5. The boundaries are influenced by the transverse strain ratio of cracked and crushed material which is expected when the failure criterion is based on principal strains. This disadvantage of the presented model can be solved by defining the dependence between tensile and compressive strength. Nevertheless, the real shape of failure envelope for SHCC will only be included at a later stage as the biaxial behavior is currently under investigation at Stellenbosch University.

2.4. Cyclic loading

The above described model is adjusted for cyclic loading when the orientation of principle stresses changes. The residual deformations are assumed to be dependant on the inelastic strain. Therefore,

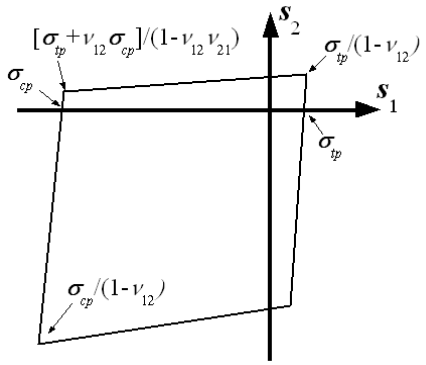

Fig. 5: Failure envelope in the principal stress space

a simple linear definition is employed and the permissible closing (opening) strain is evaluated as

$$\varepsilon_{t(c)}^{cl} = b_{t(c)}^{cl} \varepsilon_{tul(cul)}, \tag{28}$$

where b_t^{cl} and b_c^{cl} are material parameters and can therefore be calculated from reverse cyclic loading tests. The trajectories of reloading after the stress state change are in a good agreement with experimental results presented in (Billington, 2004).

For the space limitation only tension behavior after stress state change is introduced (Eqs. (29,30)). The stress evolution for compression can be obtain by substitution of tensile driving parameters for compressive variables and replacement of the maximum (max) with the minimum (min) value and vice versa. Note that during the loading after stress state change the old cracks are reopened and the tangent modulus increases to reach the value of the previously experienced modulus E_t.

$$\sigma\left(\dot{e} \geq 0\right) = \sigma_{tul}^{*} + \left(\sigma_{tmax}^{**} - \sigma_{tul}^{*}\right) \left(\frac{\hat{e} - \varepsilon_{tul}^{*}}{\varepsilon_{tmax}^{**} - \varepsilon_{tul}^{*}} \right)^{E_t \frac{\varepsilon_{tmax}^{**} - \varepsilon_{tul}^{*}}{\sigma_{tmax}^{**} - \sigma_{tul}^{*}}}, \tag{29}$$

$$\sigma\left(\dot{e} < 0\right) = \sigma_{tmax}^{*} \left[\frac{\hat{e} - \varepsilon_{tul}^{**}}{\sigma_{tmax}^{*} / E_t} \right]^{a_t}, \tag{30}$$

where the driving parameter $\hat{e}$ is again shifted to correspond with the diagram for a virgin loading and $\varepsilon_{tmax}^{**} = \max\left(\varepsilon_{t0}, \varepsilon_{tmax}\right)$ with associated stress σ_{tmax}^{**}. The experienced modulus is determined as

$$E_t = \begin{cases} E_0 & \varepsilon_{tmax} \leq \varepsilon_{t0} \quad (31) \\ \dfrac{\sigma_{tmax}}{\varepsilon_{tmax} - b_t\left(\varepsilon_{tmax} - \varepsilon_{t0}\right)} & \varepsilon_{tmax} > \varepsilon_{t0}, \quad (32) \end{cases}$$

and inelastic strain ε_{tul}^{**} is assumed to be

$$\varepsilon_{tul}^{**} = \min\left[\varepsilon_{tmax}^{*} - \sigma_{tmax}^{*} / E_t, b_t\left(\varepsilon_{tmax} - \varepsilon_{t0}\right)\right]. \tag{33}$$

To demonstrate the model response, a loading change from tension to compression to tension (A-G) is shown in Fig. 6(a):

- A-B: initial virgin loading (Eq. (14)),
- B-C: unloading (Eq. (15)),
- C-D: cracks closing and compressive loading,
- D-E: virgin loading (Eq. (22)),

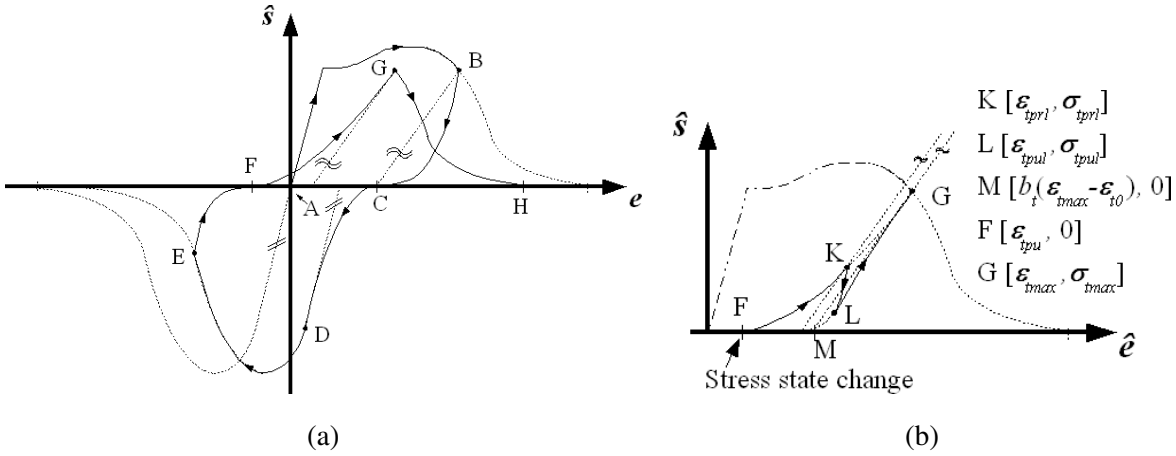

(a) (b)

Fig. 6: Schematic cyclic behavior

- E-F: unloading (Eq. (23)),
- F-G: cracks reopening and tensile loading (Eq. (29)),
- G-H: virgin loading (Eq. (14)).

Note that if the loading follows the stress state change, the loading path has the tangent equal to the actual modulus (Eq. (29)), intervals F-K and L-G in Fig. 6(b). The unloading from this stage is defined in Eq. (30), see interval K-L in Fig. 6(b).

3. Implementation and application

As mentioned in the previous section, the constitutive model is implemented in the commercial available finite element code **DIANA** version 9.3 using the "User supplied subroutine" option to demonstrate its suitability for SHCC. Note that this section is brief demonstration. Therefore, a more wide and deep study is preparing by the authors and will be presented separately. The Newton-Raphson iterative procedure is used for the solution of nonlinear equations.

Finite element analyses of the flexural tests is performed to verify the constitutive model analyses. The three-point bending test is introduced using parameters based on the tensile tests and data presented by Boshoff (2007). The obtained results are compared with experimental data.

3.1. Model description

The numerical model is based on experimental data obtained over the past 5 years by the Institute of Structural Engineering based at the Department of Civil Engineering, Stellenbosch University. Due to the lack of a reverse cyclic loading some parameters are set up using the engineering judgement of the authors as this will not have a significant influence on the presented results. The available tensile tests for the same mixture as beams are used to set up the parameters describing tension, see Fig. 7(a). All the model parameters are listed in Tab. 1. To examine the feasibility of the proposed numerical approach, two different meshes are used. The flexural test is modelled using four node quadrilateral isoparametric plane stress element Q8MEM which are based on linear interpolation and Gauss integration. Two by two integration scheme is set up.

The finite element mesh is refined towards the middle of the beam with the size of the elements in the expected softening and localization zone 1.33 mm x 1.33 mm and 4.0 x 4.0 mm. The former dimension of elements in the middle of the beam is chosen in accordance with the theory introduced in (Boshoff, 2007) to deal with the crack spacing. The boundary conditions of the model are shown in Fig. 7(b) as well as the beam dimensions. The other mesh size is chosen to study the mesh sensitivity.

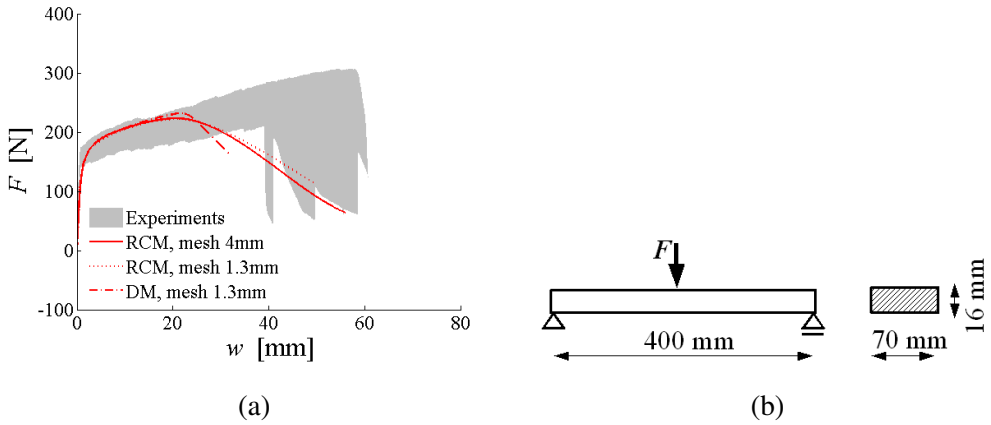

Fig. 7: Three-point bending test: (a) Comparison, (b) setup setup

Tab. 1: Model parameters

General			Tension		Compression	
Param.	Value		Param.	Value	Param.	Value
E	9200	MPa	ε_{t0}	$2.42 \cdot 10^{-4}$	ε_{c0}	$-4.89 \cdot 10^{-3}$
ν	0.35		ε_{tp}	$3.92 \cdot 10^{-2}$	ε_{cp}	$-5.89 \cdot 10^{-3}$
			σ_{tp}	2.79 MPa	σ_{cp}	-50.0 MPa
			w_t	6.0 mm	ε_{cu}	$-2.00 \cdot 10^{-1}$
			a_t	3.0	d_c	50 mm
			b_t	0.8	a_c	3.0
			b_t^{cl}	0.6	b_c	0.8
					b_c^{cl}	0.8

3.2. Results

The presented crack rotating model (RCM) is used to obtain the force-deflection diagrams. These results are plotted in Fig. 7(a) together with the experimental data and response produced by the model based on a damage mechanics formulation (DM) by Boshoff (2007). As can be seen, the numerical models demonstrate good agreement with experimental data in the elastic as well as hardening part. The discrepancy is detected for the softening part. This is probably caused by the fibers alignment close to the surface which is not taken into account for generally used numerical models and the interested readers are referred to (Boshoff, 2007). The mesh dependency is observed by comparison of the two different mesh sizes.

4. Conclusion and future work

In this paper a two-dimensional numerical model for Strain Hardening Cement-based Composites was introduced. This approach is based on a rotating crack model implemented in the commercially available software package **DIANA**. The presented model takes into account:

- strain hardening and softening in tension as well as in compression,
- nonlinear unloading,
- nonlinear loading after stress state change - crack closing,
- the effect of Poisson's ratio.

The accuracy of the introduced approach was demonstrated by means of a three-point flexural test. Nevertheless, the model must be further verified before the proposed approach will be used for larger structural components under different loading conditions.

Acknowledgment

The financial support provided by the GAČR grant No. 105/12/P353 is gratefully acknowledged.

References

Billington S (2004). Damage-tolerant cement-based materials for performence-based erthquake engineering design: Research needs, *in Fracture Mechanics of Concrete Structures*, pp. 53–60.

Boshoff W (2007), Time-Dependant Behaviour of Engineered Cement-Based Composites, PhD thesis, University of Stellenbosch. Ph.D. thesis.

Boshoff W, Mechtcherine V and van Zijl G (2009*a*). Characterising the time-dependant behaviour on the single fibre level of SHCC: Part 1: Mechanism of fibre pull-out creep, *Cement and Concrete Research* **39**, 779–786.

Boshoff W, Mechtcherine V and van Zijl G (2009*b*). Characterising the time-dependant behaviour on the single fibre level of SHCC: Part 2: The rate effects on fibre pull-out tests, *Cement and Concrete Research* **39**, 787–797.

Boshoff W and van Zijl G (2007). Time-dependant response of ECC: Characterisation of creep and rate dependence, *Cement and Concrete Research* **37**, 725–734.

BV. T D (2008). *DIANA Finite Element Analysis*.

Han T S, Feenstra P and Billington S (2003). Simulation of Highly Ductile Fiber-Reinforced Cement-Based Composite Components Under Cyclic Loading, *ACI Structural Journal* **100**(6), 749–757.

Jirásek M and Zimmermann Z (1998). Analysis of Rotating Crack Model, *Journal of Engineering Mechanics* **124**(8), 842–851.

Kabele P (2000), Assessment of Structural Performance of Engineered Cemetitious Composites by Computer Simulation, PhD thesis, Czech Technical University in Prague. A habilitation thesis.

Li V and Wang S (2001). Tensile Strain-hardening Behavior of PVA-ECC, *ACI Materials Journal* **98**(6), 483–492.

Mechtcherine V and Jůn P (2007). Stress-strain behaviour of strain-hardening cement-based composites (SHCC) under repeated tensile loading, *in Fracture Mechanics of Concrete Structures*, pp. 1441–1448.

Rots J (1998), Computational modeling of concrete fracture, PhD thesis, Delft University of Technology. Ph.D. thesis.

Simone A, Sluys L and Kabele P (2003). Combined continuous/discontinuous failure of cementitious composites, *in Proceedings for EURO-C 2003: Computational Modelling of Concrete Structures*, pp. 133–137.

Suryanto B, Nagai K and Maekawa K (2008). Influence of damage on cracking behavior of ductile fibre-reinforced cementitious composite, *in Proceedings of 8th International Conference on Creep, Shrinkage and Durability of Concrete and Concrete Structures*, pp. 495–500.